

Channel Estimation for Beyond Diagonal RIS

Exploiting Core Tensor Sparsity

Daniel Costa Araújo and André L. F. de Almeida

Abstract

Beyond diagonal reconfigurable intelligent surfaces (BD-RISs) enhance wave manipulation through inter-element couplings but pose significant channel estimation challenges due to cascaded channels and block-Kronecker structures. This paper proposes a compressive sensing framework exploiting the sparse Tucker decomposition of the measurement tensor and the Kronecker rank-one structure of channel components. Two algorithms are developed: Sparse Tensor Orthogonal Recovery Method (STORM), which uses orthogonal matching pursuit (OMP) for greedy support recovery, and Sparse Tensor subspace-Aided Recovery (STAR), which leverages subspace-based projection to enhance robustness to noise. Both perform joint sparse support identification, followed by a Kronecker rank-one factorization via singular value decomposition (SVD) to recover the channel parameters. Simulations show that STAR achieves oracle-assisted least squares (LS) performance at moderate-to-high signal-to-noise ratio (SNR) with significantly fewer measurements than baseline methods, enabling practical BD-RIS deployment in next-generation millimeter wave (mmWave)/sub-terahertz (sub-THz) networks.

Index Terms

BD-RIS, compressive sensing (CS), mmWave, reconfigurable intelligent surface (RIS)

I. INTRODUCTION

Reconfigurable intelligent surfaces (RISs) have emerged as a transformative technology for sixth-generation (6G) wireless networks, enabling programmable control of electromagnetic wave propagation through planar arrays of low-cost passive elements [1]–[4]. By dynamically adjusting the phase shifts induced by individual surface elements, conventional RISs can perform passive beamforming, enhance coverage, and improve spectral efficiency without requiring active radio-frequency chains [5]–[7]. However, the diagonal scattering matrix structure of conventional RISs, where each element operates independently, fundamentally constrains their wave manipulation flexibility [8].

BD-RISs overcome this limitation by introducing inter-element connections through reconfigurable impedance networks, yielding scattering matrices with non-zero off-diagonal entries [8], [9]. This architectural innovation enables waves absorbed by one element to propagate into neighboring elements, thereby expanding the degrees of freedom for channel engineering [10], [11]. The group-connected architecture organizes elements into groups with tunable intra-group couplings, offering a practical trade-off between performance and hardware complexity [12]. These advances translate into performance improvements, including multi-sector operation for full-space coverage [9] and superior channel gain [11], [13].

Despite these promising advantages, acquiring accurate channel state information (CSI) for BD-RIS-assisted systems is fundamentally more challenging than for conventional RIS due to several factors: (i) the passive nature of RIS elements precludes active pilot processing, necessitating estimation of cascaded transmitter-RIS-receiver channels [14]–[17]; (ii) the inter-element coupling inherent in BD-RIS architectures introduces additional structural constraints that must be leveraged for efficient estimation [18], [19]; and (iii) the large number of RIS elements, particularly in mmWave and sub-THz deployments, leads to prohibitive training overhead if not properly addressed [20].

Recent research has proposed various approaches to tackle these challenges. LS-based methods with optimized pilot sequences minimize estimation error under BD-RIS architectural constraints but require substantial training overhead [18]. Decoupled estimation techniques exploit the block structure of BD-RIS scattering matrices, reducing problem dimensionality at the cost of potential information loss [19]. Semi-blind methods based on PARATUCK tensor decomposition jointly estimate channels and data symbols, avoiding dedicated pilot overhead but with increased algorithmic complexity [21]. More recently, block Tucker decomposition has been applied to BD-RIS channel estimation, yielding performance gains over matrix-based LS methods due to its inherent noise-rejection properties [20].

Motivated by the limited-scattering nature of high-frequency propagation, typical of mmWave/sub-THz deployments where a BD-RIS restores blocked base station (BS)-user equipment (UE) coverage, CS-based methods have demonstrated significant reductions in training overhead for conventional RIS systems by exploiting channel sparsity in angular domains. For instance, the TRICE framework combines tensor decomposition with ESPRIT-based direction estimation to efficiently recover sparse channels [22]. Other techniques such as OMP leverage common support across users and subcarriers to recover sparse channel representations with reduced pilot se-

quences [23], while deep learning-enhanced CS methods further improve recovery accuracy [24]. Nevertheless, direct application of existing CS methods designed for conventional RIS to BD-RIS fails because the block-diagonal scattering structure introduces a unique sparsity pattern in the core tensor that is not captured by standard sparse recovery algorithms.

This paper proposes two novel CS-based algorithms for BD-RIS channel estimation that exploit core tensor sparsity. Both algorithms operate in two stages: first, a sparse support recovery stage identifies active propagation paths using Fourier dictionary matrices; second, a channel parameter estimation stage exploits the Kronecker rank-one structure of each support component through SVD and subspace projection to refine the estimates. Our contributions are:

- We propose a BD-RIS channel-estimation scheme that jointly compresses the transmitter, receiver, and BD-RIS training dimensions, operating in a regime in which full-dimensional tensor estimators are not identifiable.
- We formulate BD-RIS channel estimation as a sparse core-tensor recovery problem and instantiate it via STORM (greedy OMP) and STAR (subspace MUSIC).
- Through extensive simulations, we demonstrate that STAR achieves oracle performance at high SNR while requiring significantly fewer training frames than conventional methods, with computational complexity lower than the TRICE framework [22] adapted to BD-RIS.

II. SYSTEM MODEL

We consider a RIS-assisted system comprising a BS with N antennas, a RIS with K elements, and a UE with M antennas. The RIS adopts a BD-RIS architecture with Q groups of \bar{K} elements each, where $K = \bar{K}Q$. During training, beam matrices $\mathbf{W}_{\text{tx}} \in \mathbb{C}^{N \times N_{\text{tx}}}$ and $\mathbf{W}_{\text{rx}} \in \mathbb{C}^{M \times M_{\text{rx}}}$ are employed, with $N_{\text{tx}} \ll N$ and $M_{\text{rx}} \ll M$, a regime under which the full-dimensional tensor estimator of [20] is not identifiable. Let $\mathbf{G} \in \mathbb{C}^{N \times K}$ and $\mathbf{H} \in \mathbb{C}^{M \times K}$ denote the BS-RIS and UE-RIS channels. For the ℓ -th training frame, each group q has scattering matrix $\mathbf{W}_{\text{ris}}^{(q,\ell)} \in \mathbb{C}^{\bar{K} \times \bar{K}}$, forming the block diagonal matrix

$$\mathbf{B}^{(\ell)} = \text{blkdiag} \left[\mathbf{W}_{\text{ris}}^{(1,\ell)}, \dots, \mathbf{W}_{\text{ris}}^{(Q,\ell)} \right]. \quad (1)$$

Consider $\mathbf{H}_q, \mathbf{G}_q$ as the column sub-matrices of \mathbf{H}, \mathbf{G} for the \bar{K} elements of group q . With the processed channels $\bar{\mathbf{H}}_q = \mathbf{W}_{\text{rx}} \mathbf{H}_q \in \mathbb{C}^{M_{\text{rx}} \times \bar{K}}$ and $\bar{\mathbf{G}}_q = \mathbf{W}_{\text{tx}} \mathbf{G}_q \in \mathbb{C}^{N_{\text{tx}} \times \bar{K}}$, the signal during frame ℓ is

$$\mathbf{Y}^{(\ell)} = \sum_{q=1}^Q \bar{\mathbf{H}}_q \mathbf{W}_{\text{ris}}^{(q,\ell)} \bar{\mathbf{G}}_q^T + \mathbf{N}^{(\ell)}, \quad (2)$$

where $\mathbf{N}^{(\ell)}$ is the processed noise matrix. The channels are modeled as $\mathbf{H} = \mathbf{U}_H \mathbf{\Lambda}_H \mathbf{V}_H^H$ and $\mathbf{G} = \mathbf{U}_G \mathbf{\Lambda}_G \mathbf{V}_G^H$, where $\mathbf{U}_H, \mathbf{U}_G$ contain steering vectors at UE and BS, $\mathbf{V}_H, \mathbf{V}_G$ at the RIS, and $\mathbf{\Lambda}_H, \mathbf{\Lambda}_G$ are diagonal path gain matrices with P paths each, set to $P_G = P_H = P$ for notational simplicity, with the framework extending to $P_G \neq P_H$ via sparsity $S = P_G P_H$. Owing to limited mmWave/sub-THz scattering, P is small and each link is angularly sparse. We introduce the block Kronecker product operator $\mathbf{A} | \otimes | \mathbf{B} = [\mathbf{A}_1 \otimes \mathbf{B}_1, \dots, \mathbf{A}_Q \otimes \mathbf{B}_Q]$ and define $\bar{\mathbf{V}} = \mathbf{V}_G^H | \otimes | \mathbf{V}_H^H$. By vectorizing (2) and concatenating all K_{ris} training frames, while collecting the vectorized RIS configurations as $\mathbf{w}_{\text{ris}}^{(\ell)} = [\text{vec}(\mathbf{W}_{\text{ris}}^{(1,\ell)})^T, \dots, \text{vec}(\mathbf{W}_{\text{ris}}^{(Q,\ell)})^T]^T$ into $\mathbf{W}_{\text{ris}} = [\mathbf{w}_{\text{ris}}^{(1)}, \dots, \mathbf{w}_{\text{ris}}^{(K_{\text{ris}})}] \in \mathbb{C}^{Q\bar{K}^2 \times K_{\text{ris}}}$, the noise-free received signal across all frames becomes $\mathbf{X} = (\mathbf{W}_{\text{tx}} \mathbf{U}_G \otimes \mathbf{W}_{\text{rx}} \mathbf{U}_H) (\mathbf{\Lambda}_G \otimes \mathbf{\Lambda}_H) \bar{\mathbf{V}} \mathbf{W}_{\text{ris}}$, with $\mathbf{X} = [\text{vec}(\mathbf{X}^{(1)}), \dots, \text{vec}(\mathbf{X}^{(K_{\text{ris}})})]$. Taking the transpose reveals a Tucker-3 structure:

$$\mathbf{X}^T = \mathbf{A}_3 \mathbf{D}_{(3)} (\mathbf{A}_2 \otimes \mathbf{A}_1)^T, \quad (3)$$

where $\mathbf{A}_1 = \mathbf{W}_{\text{tx}} \mathbf{U}_G \in \mathbb{C}^{N_{\text{tx}} \times P}$, $\mathbf{A}_2 = \mathbf{W}_{\text{rx}} \mathbf{U}_H \in \mathbb{C}^{M_{\text{rx}} \times P}$, $\mathbf{A}_3 = \mathbf{W}_{\text{ris}}^T \bar{\mathbf{V}}^T \in \mathbb{C}^{K_{\text{ris}} \times P^2}$, and $\mathbf{D}_{(3)} = (\mathbf{\Lambda}_G \otimes \mathbf{\Lambda}_H)^T$ is the mode-3 unfolding of the core tensor \mathcal{D} . The tensor model is $\mathcal{Y} = \mathcal{X} + \mathcal{N}$, where $\mathcal{Y}, \mathcal{X}, \mathcal{N} \in \mathbb{C}^{N_{\text{tx}} \times M_{\text{rx}} \times K_{\text{ris}}}$.

A conventional LS approach requires $K_{\text{ris}} > Q\bar{K}^2$ frames for identifiability, which becomes prohibitive as \bar{K} grows [20]. However, in mmWave/sub-THz scenarios, $P \ll K$, so \mathcal{D} is sparse and can be recovered with far fewer measurements through CS techniques.

III. PROPOSED CHANNEL ESTIMATION

We propose a CS-based channel estimation algorithm that exploits the sparsity structure of the core tensor \mathcal{D} in (3). The proposed approach consists of two main stages: sparse support recovery and channel parameter estimation.

A. Stage 1: Sparse Support Recovery

We construct discrete Fourier transform (DFT) dictionary matrices $\mathbf{F}_1 \in \mathbb{C}^{N \times N_{\text{grid}}}$, $\mathbf{F}_2 \in \mathbb{C}^{M \times N_{\text{grid}}}$, $\mathbf{F}_G, \mathbf{F}_H \in \mathbb{C}^{K \times N_{\text{grid}}}$, and $\mathbf{F}_3 = (\mathbf{F}_G^H | \otimes | \mathbf{F}_H^H) \in \mathbb{C}^{Q\bar{K}^2 \times N_{\text{grid}}^2}$, all discretizing the respective array steering vectors on N_{grid} bins. Defining $\bar{\mathbf{A}}_1 = \mathbf{W}_{\text{tx}} \mathbf{F}_1$, $\bar{\mathbf{A}}_2 = \mathbf{W}_{\text{rx}} \mathbf{F}_2$, and $\bar{\mathbf{A}}_3 = \mathbf{W}_{\text{ris}}^T \mathbf{F}_3$, the CS problem is

$$\mathbf{X}_{(3)}^T = \bar{\mathbf{A}}_3 \boldsymbol{\theta} + \mathbf{N}_{(3)}^T, \quad (4)$$

where $\boldsymbol{\theta} \in \mathbb{C}^{N_{\text{grid}}^2 \times N_{\text{tx}} M_{\text{rx}}}$ is row-sparse with P^2 non-zero rows indexed by the active (p_G, p_H) pairs, each of the form $d_s(\bar{\mathbf{A}}_2 \otimes \bar{\mathbf{A}}_1)(:, s)^T$ so that the TX/RX dictionaries are exposed only in the Stage 2 reshape. We propose two strategies:

STORM (OMP-based): Applies OMP to (4) using $\bar{\mathbf{A}}_3$ as dictionary, iteratively selecting atoms with maximum residual correlation over $S = |\mathcal{S}|$ iterations.

STAR (Subspace-based): Computes the SVD of $\mathbf{X}_{(3)}^T$ and identifies the support via the MUSIC-like spectrum

$$\hat{s} = \arg \min_{k \in \{1, \dots, N_{\text{grid}}^2\}} \|\bar{\mathbf{A}}_3(:, k)^H \mathbf{U}_{\text{null}}\|_F^2, \quad (5)$$

selecting the S indices with the smallest noise-subspace projection. For both methods, once \mathcal{S} is determined, the coefficients are estimated via $\hat{\boldsymbol{\theta}}_{\mathcal{S}} = \bar{\mathbf{A}}_{3, \mathcal{S}}^\dagger \mathbf{X}_{(3)}^T$.

B. Stage 2: Channel Parameter Estimation

For each support index $s \in \mathcal{S}$, the row $\hat{\boldsymbol{\theta}}_{s, \cdot}$ of length $N_{\text{tx}} M_{\text{rx}}$ is reshaped column-wise into $\mathbf{M}_s = \text{unvec}_{N_{\text{tx}} \times M_{\text{rx}}}(\hat{\boldsymbol{\theta}}_{s, \cdot}^T) \in \mathbb{C}^{N_{\text{tx}} \times M_{\text{rx}}}$, which is rank-one because each non-zero row of $\boldsymbol{\theta}$ corresponds to a single path pair (p_G, p_H) :

$$\mathbf{M}_s = \mathbf{A}_1(:, p_G) \mathbf{A}_2(:, p_H)^T. \quad (6)$$

Since s encodes (p_G, p_H) , no path-pair matching is needed, and off-grid leakage is mitigated by oversampled dictionaries.

Performing SVD on $\mathbf{M}_s = \mathbf{U}_s \boldsymbol{\Sigma}_s \mathbf{V}_s^H$ and defining noise subspaces \mathbf{U}_{null} and \mathbf{V}_{null} from the trailing $(N_{\text{tx}} - 1)$ and $(M_{\text{rx}} - 1)$ singular vectors of \mathbf{U}_s and \mathbf{V}_s , respectively, we estimate the path indices via

$$\begin{aligned} \hat{p}_{\text{tx}} &= \arg \min_i \|\bar{\mathbf{A}}_1(:, i)^H \mathbf{U}_{\text{null}}\|_F^2, \\ \hat{p}_{\text{rx}} &= \arg \min_j \|\bar{\mathbf{A}}_2(:, j)^T \mathbf{V}_{\text{null}}\|_F^2, \end{aligned} \quad (7)$$

and compute $\hat{d}_s = \bar{\mathbf{A}}_1(:, \hat{p}_{\text{tx}})^H \mathbf{M}_s \bar{\mathbf{A}}_2(:, \hat{p}_{\text{rx}})^*$. After processing all $s \in \mathcal{S}$, the entries \hat{d}_s form $\hat{\mathbf{D}}_{(3), \mathcal{S}} = \text{diag}(\hat{d}_1, \dots, \hat{d}_{|\mathcal{S}|})$ and the composite channel is

$$\widehat{\mathbf{G}} \otimes \widehat{\mathbf{H}} = \mathbf{F}_{3, \mathcal{S}} \hat{\mathbf{D}}_{(3), \mathcal{S}} (\mathbf{F}_{2, \mathcal{S}} \otimes \mathbf{F}_{1, \mathcal{S}})^T. \quad (8)$$

Algorithms 1 and 2 summarize the complete procedures for STORM and STAR, highlighting the Stage 1 difference that governs the performance trade-off between the two methods.

Algorithm 1 STORM: OMP-based sparse tensor recovery

Require: $\mathbf{X}_{(3)}^T$, dictionaries $\bar{\mathbf{A}}_1, \bar{\mathbf{A}}_2, \bar{\mathbf{A}}_3$, sparsity S
Ensure: Estimated composite channel $\widehat{\mathbf{G}} \otimes \widehat{\mathbf{H}}$
Stage 1: OMP-based support recovery

- 1: $\mathcal{S} \leftarrow \emptyset, \mathbf{R} \leftarrow \mathbf{X}_{(3)}^T$
- 2: **for** $t = 1, \dots, S$ **do**
- 3: $k^* \leftarrow \arg \max_k \|\bar{\mathbf{A}}_3(:, k)^H \mathbf{R}\|_F$ ▷ correlation
- 4: $\mathcal{S} \leftarrow \mathcal{S} \cup \{k^*\}$
- 5: $\hat{\boldsymbol{\theta}}_{\mathcal{S}} \leftarrow \bar{\mathbf{A}}_{3, \mathcal{S}}^\dagger \mathbf{X}_{(3)}^T$ ▷ LS update
- 6: $\mathbf{R} \leftarrow \mathbf{X}_{(3)}^T - \bar{\mathbf{A}}_{3, \mathcal{S}} \hat{\boldsymbol{\theta}}_{\mathcal{S}}$ ▷ residual update
- 7: **end for**

Stage 2: Kronecker rank-one factorization

- 8: **for each** $s \in \mathcal{S}$ **do**
 - 9: Reshape $\hat{\boldsymbol{\theta}}_{\mathcal{S}(s),:}^T$ into $\mathbf{M}_s \in \mathbb{C}^{N_{\text{tx}} \times M_{\text{rx}}}$
 - 10: $[\mathbf{U}_s, \boldsymbol{\Sigma}_s, \mathbf{V}_s] \leftarrow \text{SVD}(\mathbf{M}_s)$
 - 11: $\mathbf{U}_{\text{null}}^{(s)} \leftarrow$ trailing $(N_{\text{tx}} - 1)$ cols. of \mathbf{U}_s
 - 12: $\mathbf{V}_{\text{null}}^{(s)} \leftarrow$ trailing $(M_{\text{rx}} - 1)$ cols. of \mathbf{V}_s
 - 13: Estimate $\hat{p}_{\text{tx}}, \hat{p}_{\text{rx}}$ via (7)
 - 14: $\hat{d}_s \leftarrow \bar{\mathbf{A}}_1(:, \hat{p}_{\text{tx}})^H \mathbf{M}_s \bar{\mathbf{A}}_2(:, \hat{p}_{\text{rx}})^*$
 - 15: **end for**
 - 16: $\hat{\mathbf{D}}_{(3), \mathcal{S}} \leftarrow \text{diag}(\hat{d}_1, \dots, \hat{d}_{|\mathcal{S}|})$
 - 17: **return** $\mathbf{F}_{3, \mathcal{S}} \hat{\mathbf{D}}_{(3), \mathcal{S}} (\mathbf{F}_{2, \mathcal{S}} \otimes \mathbf{F}_{1, \mathcal{S}})^T$
-

TABLE I
COMPUTATIONAL COMPLEXITY COMPARISON

Method	Stage 1	Stage 2
STORM	$\mathcal{O}(SK_{\text{ris}} N_{\text{grid}}^2 N_{\text{tx}} M_{\text{rx}})$	$\mathcal{O}(SN_{\text{grid}}(N_{\text{tx}}^2 + M_{\text{rx}}^2))$
STAR	$\mathcal{O}(K_{\text{ris}}^2 (N_{\text{grid}}^2 + N_{\text{tx}} M_{\text{rx}}))$	$\mathcal{O}(SN_{\text{grid}}(N_{\text{tx}}^2 + M_{\text{rx}}^2))$
Vectorised CS	$\mathcal{O}(SK_{\text{ris}} N_{\text{tx}} M_{\text{rx}} N_{\text{grid}}^4)$	—
TRICE [22]	$\mathcal{O}(K_{\text{ris}}^2 Q \bar{K}^2 N_{\text{tx}} M_{\text{rx}})$	$\mathcal{O}(K_{\text{ris}} Q \bar{K}^2)$

Algorithm 2 STAR: Subspace-based sparse tensor recovery

Require: $\mathbf{X}_{(3)}^T$, dictionaries $\bar{\mathbf{A}}_1, \bar{\mathbf{A}}_2, \bar{\mathbf{A}}_3$, sparsity S

Ensure: Estimated composite channel $\widehat{\mathbf{G}} \otimes \widehat{\mathbf{H}}$

Stage 1: Subspace-based support recovery

- 1: $[\mathbf{U}, \boldsymbol{\Sigma}, \mathbf{V}] \leftarrow \text{SVD}(\mathbf{X}_{(3)}^T)$
- 2: $\mathbf{U}_{\text{null}} \leftarrow$ trailing $(K_{\text{ris}} - S)$ columns of \mathbf{U}
- 3: **for** $k = 1, \dots, N_{\text{grid}}^2$ **do**
- 4: $f(k) \leftarrow \|\bar{\mathbf{A}}_3(:, k)^H \mathbf{U}_{\text{null}}\|_F^2$ ▷ MUSIC spectrum
- 5: **end for**
- 6: $\mathcal{S} \leftarrow$ indices of the S smallest $f(k)$
- 7: $\hat{\boldsymbol{\theta}}_{\mathcal{S}} \leftarrow \bar{\mathbf{A}}_{3,\mathcal{S}}^\dagger \mathbf{X}_{(3)}^T$

Stage 2: Execute Stage 2 of Algorithm 1 (Steps 8–14)

C. Computational Complexity Analysis

We analyze the floating-point complexity of STORM and STAR. Let $S = |\mathcal{S}|$, N_{grid} be the angle-grid size, and P the number of paths per channel.

The OMP-based support recovery in STORM runs S iterations, each dominated by the correlation $\bar{\mathbf{A}}_3^H \mathbf{R}$ at cost $\mathcal{O}(K_{\text{ris}} N_{\text{grid}}^2 N_{\text{tx}} M_{\text{rx}})$, yielding a Stage 1 complexity $\mathcal{C}_{\text{Stage 1}}^{\text{STORM}} = \mathcal{O}(S K_{\text{ris}} N_{\text{grid}}^2 N_{\text{tx}} M_{\text{rx}})$. For STAR, the Stage 1 cost is instead dominated by a single SVD of the mode-3 unfolding and by a one-shot projection of the N_{grid}^2 dictionary atoms onto the noise subspace, with total complexity $\mathcal{C}_{\text{Stage 1}}^{\text{STAR}} = \mathcal{O}(K_{\text{ris}}^2 (N_{\text{grid}}^2 + N_{\text{tx}} M_{\text{rx}}))$, independent of the support size S .

Stage 2 is identical for both STORM and STAR. For each of the S identified support indices, Stage 2 performs the following operations: (i) computing the pseudoinverse $\bar{\mathbf{A}}_{3,\mathcal{S}}^\dagger$, which has complexity $\mathcal{O}(\min(K_{\text{ris}}, S)^2 \max(K_{\text{ris}}, S))$ when computed once for the entire support set; (ii) reshaping and SVD of $\mathbf{M}_{\mathcal{S}} \in \mathbb{C}^{N_{\text{tx}} \times M_{\text{rx}}}$, with complexity $\mathcal{O}(N_{\text{tx}} M_{\text{rx}} \min(N_{\text{tx}}, M_{\text{rx}}))$ per support index; and (iii) noise subspace search over the dictionary atoms as in (7), which projects all columns of $\bar{\mathbf{A}}_1$ and $\bar{\mathbf{A}}_2$ onto the noise subspaces $\mathbf{V}_{\text{null}} \in \mathbb{C}^{N_{\text{tx}} \times (N_{\text{tx}} - 1)}$ and $\mathbf{U}_{\text{null}} \in \mathbb{C}^{M_{\text{rx}} \times (M_{\text{rx}} - 1)}$, requiring $\mathcal{O}(N_{\text{grid}}(N_{\text{tx}}^2 + M_{\text{rx}}^2))$ operations per index. Aggregating over all S support indices, the total Stage 2 complexity is $\mathcal{O}(S N_{\text{grid}}(N_{\text{tx}}^2 + M_{\text{rx}}^2))$.

Since $S \ll N_{\text{grid}}^2$ and $K_{\text{ris}} \ll Q \bar{K}^2$, the total complexity is dominated by Stage 1 for large N_{grid} . Both methods achieve lower complexity than TRICE [22], $\mathcal{O}(K_{\text{ris}}^2 Q \bar{K}^2 N_{\text{tx}} M_{\text{rx}})$, by exploiting the

Kronecker rank-one structure. The Stage 1 difference drives the trade-off: STORM uses greedy OMP, fast at high SNR, while STAR uses a MUSIC-like subspace search, more robust at low SNR. The sparsity S enters Stage 1 only for STORM, which scales linearly with S , whereas STAR is sparsity-independent in Stage 1. The shared Stage 2 grows linearly with S for both.

Table I summarizes the computational complexity comparison among different methods. As a matter of comparison, we analyse the vectorised CS approach, which applies OMP directly to the flattened tensor measurement vector of dimension $K_{\text{ris}}N_{\text{tx}}M_{\text{rx}}$, constructing a dictionary via the Khatri-Rao product $\text{KR}(\mathbf{A}_1 \otimes \mathbf{A}_2, \mathbf{A}_3)$ with N_{grid}^4 atoms, covering all possible angle combinations across the three tensor modes. This single-stage OMP approach incurs prohibitively high complexity $\mathcal{O}(SK_{\text{ris}}N_{\text{tx}}M_{\text{rx}}N_{\text{grid}}^4)$ that scales quartically with the grid size and does not benefit from the two-stage decomposition. In contrast, by exploiting the tensor structure and Kronecker factorization, STORM and STAR reduce the dictionary size from N_{grid}^4 to N_{grid}^2 , achieving a quadratic reduction in complexity. The TRICE framework, while also exploiting tensor structure, incurs a higher Stage 1 cost because it performs full tensor decomposition without exploiting core tensor sparsity. As shown in the table, STORM and STAR share identical Stage 2 complexity but differ in their Stage 1 support recovery mechanisms, with STAR providing enhanced noise robustness at the expense of a slightly higher computational cost during the support estimation phase.

IV. NUMERICAL RESULTS

We evaluate the proposed scheme through Monte Carlo simulations, reporting the normalized mean squared error (NMSE) versus SNR, the NMSE versus the fraction of RIS measurements relative to $Q\bar{K}^2$, the NMSE versus the number of paths, and the processing time versus \bar{K} . Default parameters are listed in Table II; P is assumed known and estimable in practice via classical MDL/AIC rank tests on $\mathbf{X}_{(3)}$. We compare the proposed STORM and STAR with the TRICE framework [22] adapted to BD-RIS and the LS Oracle (LSO), which knows the true support and serves as a lower bound. \mathbf{W}_{tx} , \mathbf{W}_{rx} and the per-group $\mathbf{W}_{\text{ris}}^{(q,\ell)}$ are i.i.d. complex Gaussian, with $\mathbf{W}_{\text{ris}}^{(q,\ell)}$ assembled via (1) to enforce the group-connected structure. SNR is the per-element ratio P_s/σ^2 on $\mathcal{Y} = \mathcal{X} + \mathcal{N}$ of (2), with $\mathcal{N} \sim \mathcal{CN}(0, \sigma^2\mathbf{I})$, and the path gains are $\alpha_p \sim \mathcal{CN}(0, 1/P)$. The TRICE baseline runs a joint-support OMP with sparsity $S = P^2$ over $\bar{\mathbf{A}}_2 \otimes \bar{\mathbf{A}}_1$ on the mode-2 unfolding, then a per-column sparsity-one OMP over $\bar{\mathbf{A}}_3$. The LSO solves a Khatri-Rao LS fit on the true support.

TABLE II
DEFAULT SIMULATION PARAMETERS

Parameter	Symbol	Value
BS/UE antennas	$N = M$	32
BD-RIS elements / group size	K / \bar{K}	64 / {4, 8}
TX/RX training beams	$N_{\text{tx}} = M_{\text{rx}}$	16
Paths per channel	P	2
Angular grids ($2\times$ oversampling)	$N_{\text{grid}}, N_{\text{ris,grid}}$	$2N, 2K$
SNR per element	SNR (dB)	{0, 4, ..., 20}
Monte Carlo trials per point	N_{MC}	1,000

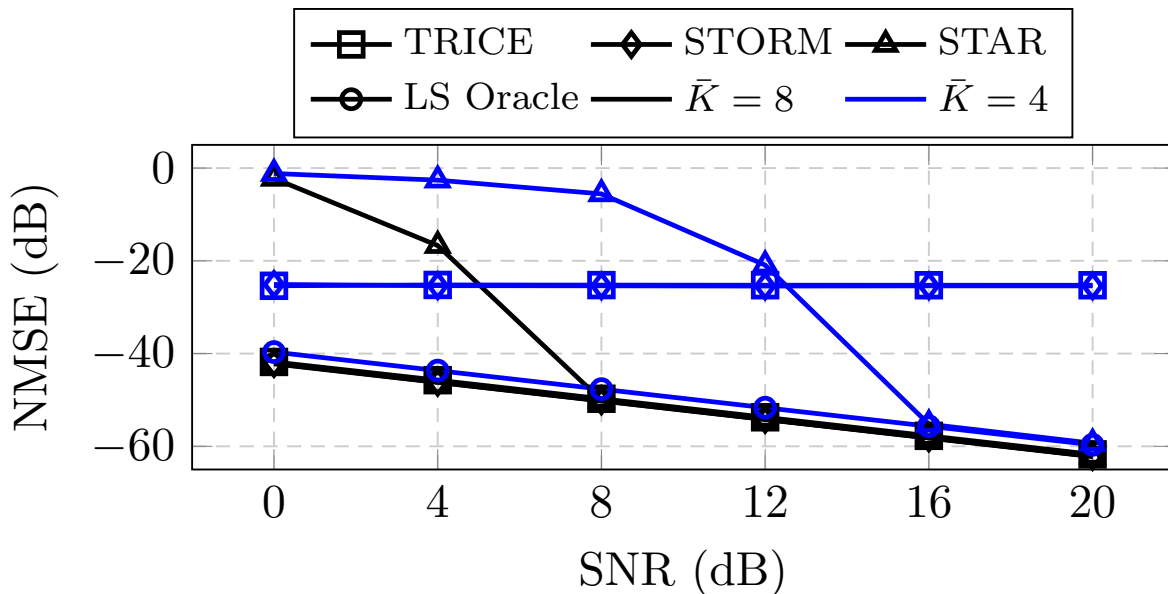


Fig. 1. NMSE as a function of SNR. Fixed: $N = 32$, $M = 32$, $K = 64$, $N_{\text{tx}} = 16$, $M_{\text{rx}} = 16$; RIS measurement size at 50% of $Q\bar{K}^2$.

Fig. 1 shows the NMSE versus SNR. The curves reflect the impact of \bar{K} : a larger \bar{K} offers greater robustness at low SNR, with a smaller NMSE gap to the bound in that regime compared with $\bar{K} = 4$. For $\bar{K} = 8$, all algorithms converge to the LSO bound as the SNR increases, confirming that the measurement budget at 50% compression is sufficient for accurate sparse recovery when the group size provides enough diversity. For $\bar{K} = 4$, only the subspace-based STAR attains the bound at high SNR, while the OMP-based TRICE [22] and STORM saturate at an SNR-independent floor. The smaller Kronecker dimension $\bar{K}^2 = 16$ raises atom coherence,

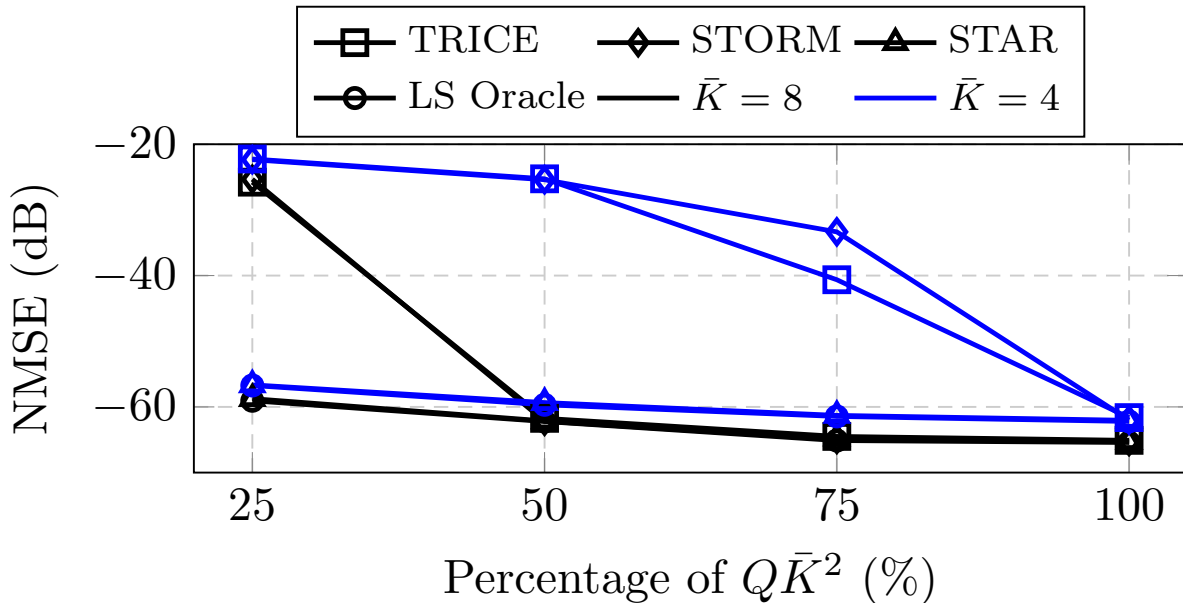


Fig. 2. NMSE as a function of the percentage of RIS measurements relative to $Q\bar{K}^2$. Fixed: $N = 32$, $M = 32$, $K = 64$, $N_{\text{tx}} = 16$, $M_{\text{rx}} = 16$.

causing OMP to misselect support atoms regardless of the noise level.

Fig. 2 plots the NMSE versus the fraction of $Q\bar{K}^2$ used as measurements, i.e., the training overhead normalized by the LS threshold $Q\bar{K}^2$. The LSO bound improves as the percentage increases due to the larger effective aperture of the measurement matrix. For $\bar{K} = 8$, all algorithms converge to the bound as the measurement fraction grows, indicating that even moderate compression ratios (30–50%) are sufficient for reliable sparse recovery. Notably, STAR achieves near-oracle performance across both group sizes: for $\bar{K} = 4$, STAR tracks the LSO bound closely even under heavy compression, whereas STORM exhibits a larger gap. This demonstrates that the subspace-based approach of STAR provides superior robustness to the reduced degrees of freedom in smaller group configurations compared to the greedy OMP-based strategy of STORM. From a practical standpoint, these results suggest that BD-RIS systems can operate with significantly fewer training frames than the $Q\bar{K}^2$ required by conventional LS methods, freeing resources for data transmission. Formal bounds for (4) follow from the coherence/spark of $\bar{\mathbf{A}}_3$ [25].

Fig. 3 shows processing time versus \bar{K} . STAR and STORM scale much more gently than TRICE, keeping larger group sizes practical and covering fully connected and hybrid BD-RIS

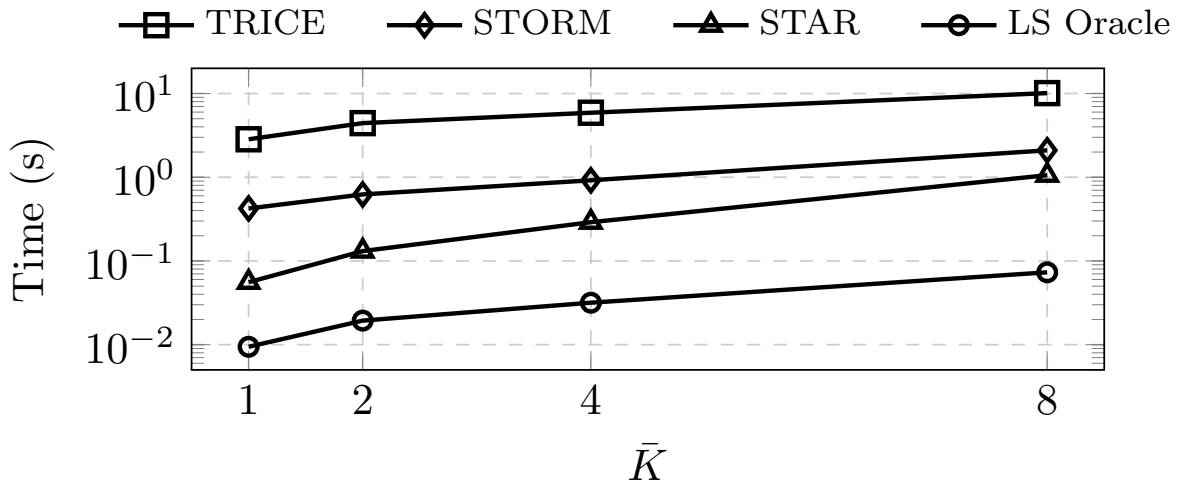


Fig. 3. Processing time of the algorithms versus \bar{K} . Fixed: $N = 32$, $M = 32$, $K = 64$, $N_{\text{rx}} = 16$, $M_{\text{rx}} = 16$; RIS measurement size at 50% of $Q\bar{K}^2$.

topologies.

Fig. 4 shows the NMSE versus the number of paths per channel with a fixed number of measurements at 50% of $Q\bar{K}^2$. As P increases, all algorithms experience performance degradation because the effective sparsity level decreases; the measurement budget remains constant while the number of unknowns grows as P^2 . This imbalance is particularly evident for STAR, which exhibits a steeper degradation curve than STORM. This behavior arises because the subspace-based support identification in STAR relies on a clear separation between the signal and noise subspaces, which degrades as the core tensor becomes less sparse. Nevertheless, for the typical path counts encountered in mmWave and sub-THz environments ($P \leq 4$), both proposed methods maintain NMSE values well below -20 dB, confirming their suitability for practical deployment. For denser-scattering scenarios, a non-sparse estimator such as the one in [20] is more appropriate.

V. CONCLUSION

This paper addressed the channel estimation problem for BD-RIS-assisted wireless systems by formulating it as a sparse core tensor recovery problem that exploits the limited-scattering properties of mmWave and sub-THz channels. The two proposed algorithms, STORM and STAR, leverage Kronecker rank-one factorization to estimate sparse channels with reduced training

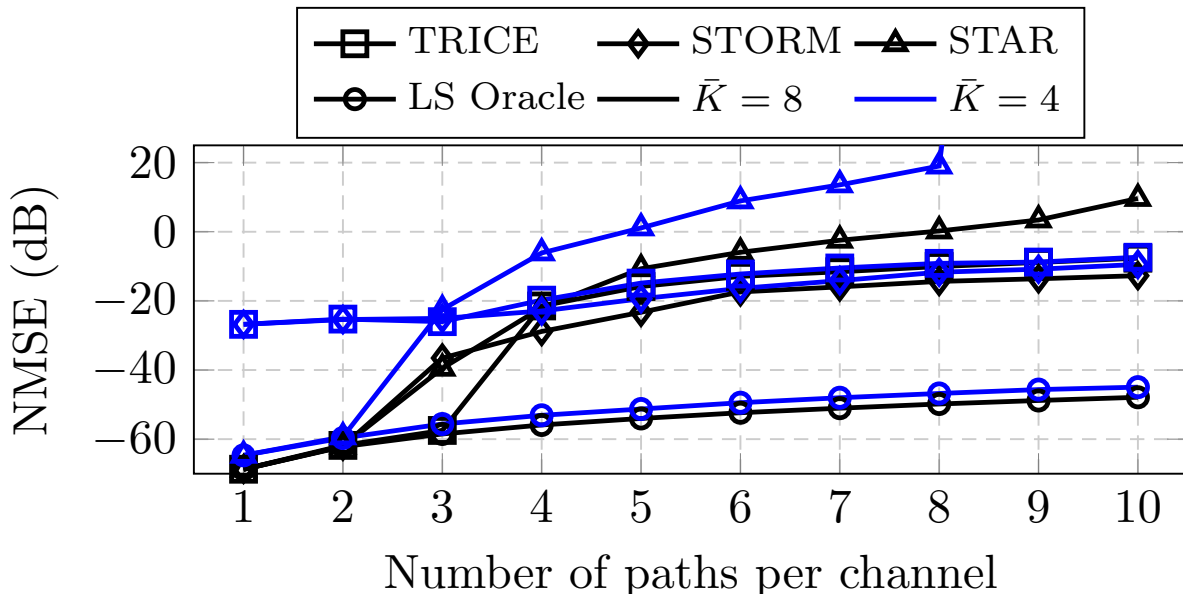


Fig. 4. NMSE as a function of the number of paths per channel. Fixed: $N = 32$, $M = 32$, $K = 64$, $N_{\text{tx}} = 16$, $M_{\text{rx}} = 16$; RIS measurement size at 50% of $Q\bar{K}^2$.

overhead, and simulations confirm near-oracle NMSE, with STAR attaining the oracle bound at high SNR while STORM and TRICE saturate at the dictionary-coherence floor for small group sizes. Both methods retain a clear complexity advantage over TRICE adapted to BD-RIS, with the largest compression gains at $\bar{K} = 8$. Future work targets wideband OFDM, hybrid group/fully-connected topologies, off-grid Stage-2 refinement, and direct-link extensions.

REFERENCES

- [1] S. Gong, X. Lu, D. T. Hoang, D. Niyato, L. Shu, D. I. Kim, and Y.-C. Liang, "Toward smart wireless communications via intelligent reflecting surfaces: A contemporary survey," *IEEE Comm. Surveys Tuts.*, vol. 22, no. 4, pp. 2283–2314, 2020.
- [2] Q. Wu, S. Zhang, B. Zheng, C. You, and R. Zhang, "Intelligent reflecting surface-aided wireless communications: A tutorial," *IEEE Trans. Comm.*, vol. 69, no. 5, pp. 3313–3351, 2021.
- [3] Y. Liu, X. Liu, X. Mu, T. Hou, J. Xu, M. Di Renzo, and N. Al-Dhahir, "Reconfigurable intelligent surfaces: Principles and opportunities," *IEEE Comm. Surveys Tuts.*, vol. 23, no. 3, pp. 1546–1577, 2021.
- [4] H. Li, M. Nerini, S. Shen, and B. Clerckx, "A tutorial on beyond-diagonal reconfigurable intelligent surfaces," *IEEE Comm. Surveys Tuts.*, vol. 28, pp. 4086–4126, 2026.
- [5] C. Huang, A. Zappone, G. C. Alexandropoulos, M. Debbah, and C. Yuen, "Reconfigurable intelligent surfaces for energy efficiency in wireless communication," *IEEE Trans. Wireless Comm.*, vol. 18, no. 8, pp. 4157–4170, 2019.
- [6] Q. Wu and R. Zhang, "Beamforming optimization for wireless network aided by intelligent reflecting surface with discrete phase shifts," *IEEE Trans. Comm.*, vol. 68, no. 3, pp. 1838–1851, 2020.
- [7] Q. Tao, Z. Li, K. Zhi, S. Li, W. Yuan, L. Zaniboni, S. Stanczak, E. Viterbo, and X. Wang, "A survey on reconfigurable intelligent surface-assisted OTFS systems," *IEEE Open J. Veh. Technol.*, vol. 6, pp. 1881–1909, 2025.
- [8] H. Li, S. Shen, M. Nerini, and B. Clerckx, "Reconfigurable intelligent surfaces 2.0: Beyond diagonal phase shift matrices," *IEEE Comm. Mag.*, vol. 62, no. 3, pp. 102–108, 2024.
- [9] H. Li, S. Shen, and B. Clerckx, "Beyond diagonal reconfigurable intelligent surfaces: A multi-sector mode enabling highly directional full-space wireless coverage," *IEEE J. Sel. Areas Comm.*, vol. 41, no. 8, pp. 2446–2460, 2023.
- [10] M. Nerini, S. Shen, H. Li, and B. Clerckx, "Beyond diagonal reconfigurable intelligent surfaces utilizing graph theory: Modeling, architecture design, and optimization," *IEEE Trans. Wireless Comm.*, vol. 23, no. 8, pp. 9972–9985, 2024.

- [11] H. Li, S. Shen, M. Nerini, M. Di Renzo, and B. Clerckx, "Beyond diagonal reconfigurable intelligent surfaces with mutual coupling: Modeling and optimization," *IEEE Comm. Lett.*, vol. 28, no. 4, pp. 937–941, 2024.
- [12] P. Del Hougne, "Physics-compliant diagonal representation of beyond-diagonal RIS," in *Proc. IEEE Int. Workshop Signal Process. Adv. Wireless Comm. (SPAWC)*, 2024, pp. 931–935.
- [13] Y. Peng, H. Li, Z. Wu, and B. Clerckx, "Lossy beyond diagonal reconfigurable intelligent surfaces: Modeling and optimization," *IEEE Trans. Wireless Comm.*, vol. 25, pp. 7365–7380, 2026.
- [14] B. Zheng, C. You, W. Mei, and R. Zhang, "A survey on channel estimation and practical passive beamforming design for intelligent reflecting surface aided wireless communications," *IEEE Comm. Surveys Tuts.*, vol. 24, no. 2, pp. 1035–1071, 2022.
- [15] A. L. Swindlehurst, G. Zhou, R. Liu, C. Pan, and M. Li, "Channel estimation with reconfigurable intelligent surfaces—a general framework," *Proc. IEEE*, vol. 110, no. 9, pp. 1312–1338, 2022.
- [16] G. T. de Araújo and A. L. F. de Almeida, "PARAFAC-based channel estimation for intelligent reflective surface assisted MIMO system," in *Proc. IEEE Sensor Array Multichannel Signal Process. Workshop (SAM)*, 2020, pp. 1–5.
- [17] G. T. de Araújo, A. L. F. de Almeida, and R. Boyer, "Channel estimation for intelligent reflecting surface assisted mimo systems: A tensor modeling approach," *IEEE J. Sel. Topics Signal Process.*, vol. 15, no. 3, pp. 789–802, 2021.
- [18] H. Li, S. Shen, Y. Zhang, and B. Clerckx, "Channel estimation and beamforming for beyond diagonal reconfigurable intelligent surfaces," *IEEE Trans. Signal Process.*, vol. 72, pp. 3318–3332, 2024.
- [19] B. Sokal, Fazal-E-Asim, A. L. F. de Almeida, H. Li, and B. Clerckx, "A decoupled channel estimation method for beyond diagonal RIS," in *Proc. Asilomar Conf. Signals, Syst., Comput.*, 2024, pp. 1395–1399.
- [20] A. L. F. de Almeida, B. Sokal, H. Li, and B. Clerckx, "Channel estimation for beyond diagonal ris via tensor decomposition," *IEEE Trans. Signal Process.*, vol. 73, pp. 4764–4779, 2025.
- [21] G. T. de Araújo and A. L. F. de Almeida, "Semi-blind channel estimation for beyond diagonal RIS," in *Proc. Asilomar Conf. Signals, Syst., Comput.*, 2024, pp. 1586–1590.
- [22] K. Ardah, S. Gherekhloo, A. L. F. de Almeida, and M. Haardt, "TRICE: A channel estimation framework for RIS-aided millimeter-wave MIMO systems," *IEEE SPL*, vol. 28, pp. 513–517, 2021.
- [23] A. Abdallah, A. Celik, M. M. Mansour, and A. M. Eltawil, "RIS-aided mmWave MIMO channel estimation using deep learning and compressive sensing," *IEEE Trans. Wireless Comm.*, vol. 22, no. 5, pp. 3503–3521, 2023.
- [24] P. M. Soumya, R. Ganiga, S. Hiremath, and M. B. Teklu, "Integration of deep learning and compressive sensing for beamspace channel estimation in mmWave massive MIMO," *IEEE Access*, vol. 13, pp. 181 200–181 216, 2025.
- [25] C. F. Caiafa and A. Cichocki, "Computing sparse representations of multidimensional signals using Kronecker bases," *Neural Comput.*, vol. 25, no. 1, pp. 186–220, 2013.